Supporting Information

Michalczyk et al. 10.1073/pnas.1502255112

Materials and Methods

Apo HCA II Preparation for Neutron Crystallography. Several preparations of wild-type HCA II were performed to obtain enough material (400 mg) for crystal growth for neutron diffraction experiments; these methods are described in detail elsewhere (1). To prepare the metal-free (*apo*) form of HCA II, the protocol described in Avvaru et al. (2) was modified as follows. The purified and concentrated enzyme was subjected to dialysis against 50 mM Tris (pH 7.5) and 100 mM 2,6-pyridine dicarboxylic acid (PDA). To achieve maximal chelation of the Zn from the active site, three or four buffer changes against this solution were done, ∼30 min apart. At these points, small aliquots of the HCA II were tested for residual esterase activity, using the *p*-nitrophenyl acetate assay (3). At the end of the last buffer change, the enzyme was over 90% inactive, indicating efficient removal of the active-site Zn. The *apo* HCA II was dialyzed against 50 mM Tris (pH 8.5) to remove any PDA.

Apo HCA II (35 mg/mL) was crystallized at room temperature for neutron experiments by mixing the protein in a 1:1 ratio with 1.15 M sodium citrate and 100 mM Tris (pH 8.5) in a 500-μL drop. The drops were equilibrated and allowed to undergo vapor exchange with a 25-mL reservoir consisting of 1.4 M sodium citrate and 100 mM Tris (pH 8.5). The crystallization drops were set up using the nine-well sandwich box setup from Hampton Research and large, single crystals appeared with 6–8 wk. Suitable *apo* HCA II crystals were selected and mounted in thick-walled quartz capillaries. After thorough wicking a liquid plug of perdeuterated mother liquor was injected next to the crystal before sealing. The crystals were left for ∼4 wk to undergo vapor H/D exchange before neutron data collection. The pH in the drops from which the crystals were harvested were checked with a microprobe pH meter and were measured to be ∼ pH 7.5. A similar crystal from the same tray was mounted and H/D-exchanged for room-temperature X-ray data collection.

Low-pH HCA II Crystal Preparation for Neutron Crystallography. Wild-type *holo* HCA II was prepared in the same way as for the *apo* form, without removal of the active-site metal. The crystallization drops were prepared in the same way as for the *apo*. When large, single crystals appeared, the pH in the drop was lowered to approximately pH 6 by adding 5 mL glacial acetic acid directly to the reservoir. The sandwich box was closed and the vapor acidified the drop. After ∼10 min the drop in pH was checked with a microprobe pH meter and was measured to be between 5.8–6.2. For mounting the crystal the following low pH H/D exchange solution was prepared in D_2O: 0.15 M sodium acetate and 1.4 M sodium citrate, pH 6. The capillary was sealed and the crystal allowed to undergo H/D exchange for 4 wk before room-temperature neutron data collection at the PCS.

Room-Temperature X-Ray and Neutron Data Collection, Structure Determination, and Refinement. Room-temperature X-ray data were collected on an in-house Rigaku HighFlux home source, equipped with 007 Micromax optics and an RAXIS-IV++ image plate detector. The instrument was operated at 40 kV and 30 mA and data were collected with a crystal–detector distance of 100 mm, 1° oscillations, and 180-s exposures. A total of 120 frames were collected to 1.60-Å resolution. Data collection and dataset statistics are shown in Table S1. Data indexing and reduction were performed using HKL3000 (4). Structure refinement against X-ray data alone was done using PHENIX Refine and manual model building in Coot (5, 6). The starting model was derived from PDB ID code 3gz0, with waters and Zn metal removed (2). After iterative rounds of manual model building and automatic refinement, the R factors converged to R_{cryst}/R_{free} of 15.7/18.2, respectively. There was ∼10% Zn metal present as determined from occupancy refinement and residual enzyme activity and was subsequently modeled as such. However, this is somewhat ambiguous as the density can readily be modeled as a water molecule also. We were unable to obtain room-temperature X-ray data of the low-pH crystal used for neutron data. For this joint refinement we used a room temperature pH 6 dataset determined previously, PDB ID code 1tbt. This is less desirable than collecting data from an H/D-exchanged crystal.

Room-temperature neutron data were collected on a large (∼2 mm^3) H/D-exchanged *apo* HCA II crystal. These data were collected at the monochromatic neutron diffractometer BIODIFF (7). This instrument is equipped with a cylindrical neutron image-plate detector (Maatel) (8). The cylindrical area detector provides large coverage of reciprocal space, thereby allowing a large number of Bragg reflections to be recorded simultaneously. The readout resolution of the image-plate scanner was set to 500 μm. The dataset was collected at room temperature. The neutron wavelength was set to 2.66 Å using a pyrolytic graphite monochromator (PG002). First, 289 frames of 0.35° rotation and 20-min exposure were recorded. To increase the completeness of the dataset the crystal was tilted by 45° from the rotation axis and a second series of 277 frames with the same rotation range and exposure time were collected. The intensities of the reflections were integrated and scaled with DENZO (v.1.96.2) and SCALEPACK (v.1.98.2) (4, 9).

For the low-pH *holo* HCA II, neutron data were collected at the PCS at LANSCE. Time-of-flight, wavelength-resolved neutron Laue diffraction images were collected at room temperature. The capillary-mounted crystal was mounted on a Huber κ-circle goniometer and 30 settings were recorded on the position sensitive ^{3}He-filled neutron detector. Each frame corresponds to 18-h exposure and corresponds to ∼22 d total beam time. Each image was processed using a version of d*TREK modified for wavelength-resolved Laue neutron protein crystallography (10, 11). The integrated reflections were wavelength-normalized using LAUENORM and then merged using SCALA incorporated into the CCP4i (12, 13). The wavelength range was restricted to 0.73–6.3 Å so as to eliminate the least accurately measured reflections. The overall completeness was ∼82% to 2.0 Å, with an R_{merge} of ∼22.8% and redundancy of 2.7 (Table 1).

In both cases the refined model from the X-ray data were used as the starting model for the joint refinement mode as implemented in nCNS, a version of CNS modified to handle simultaneous joint X-ray and neutron structure refinement (14). Before joint refinement H and D atoms (at labile positions) were generated and all H_2O molecules were replaced with D_2O molecules. Joint refinement included iterative rounds of positional, individual B factor, and occupancy refinement. Based on visual inspection of nuclear and electron density $2F_o - F_c$ and $F_o - F_c$ maps allowed for the placement of Zn and D_2O molecules as well as the positive confirmation of the protonation states of amino acid side chains, such as Tyr and His. In cases where the neutron data were not definitive, H/D atoms and solvent were oriented to accommodate H bonds and electrostatic interactions. All manual model building was done using Coot and figures were generated with PyMOL (6, 15). The last few rounds of refinement was done using Phenix Joint Refine mode using only xyz and real-space refinement options (16). The final *apo* model was refined to R_{cryst}/R_{free} of 17.9/18.8 and 20.3/21.7

for X-ray and neutron data, respectively. The final low pH *holo* model was refined to R_{cryst}/R_{free} of 20.4/21.8 and 26.3/29.1 for X-ray and neutron data, respectively. Table S1 shows a summary of the refinement statistics. Model coordinates and neutron experimental data for *apo* and *holo* have been deposited with the Protein Data Bank, with ID codes 4q49 and 4y0j, respectively.

[^{13}C]Tyr-Labeled Wild-Type HCA II Preparation for NMR pH Titration. Several ^{13}C isotopically Tyr-labeled versions of wild-type HCA II were prepared for pH titrations to ultimately determine the pK_a of Tyr7. In general, the following protocol was followed for maximal protein yield and label incorporation. Two 30-mL Luria broth (LB) (with ampicillin at 0.1 mg/mL final concentration) overnight cultures were started from BL21 glycerol stocks. These were grown at 37 °C while shaking at 225 rpm. The next morning the overnight cultures were each diluted into 1 L of fresh LB with ampicillin. The cells were grown at 37 °C while shaking at 225 rpm until the OD_{600} reached ∼1.0. At this point cells were harvested by centrifugation at 4,400 × *g* for 10 min. The cell pellets were resuspended in M9 minimal media and added to 1 L of M9 media supplemented with trace metals, 4 g glucose/L, and ampicillin. This suspension was then placed in a baffled flask and allowed to recover at 30 °C with reduced shaking at 150 rpm for about an hour. Immediately before induction of HCA II expression, the following were added to the 1 L of cell culture: 1g glyphosate and 50 mg each of Trp, Phe, and labeled Tyr. Induction of labeled protein expression was started by the addition of 1 mM (final) isopropyl-β-D-1-thiogalactopyranoside and 1 mM (final) $ZnSO_4$. Cells were grown overnight at 30 °C for ∼18 h. Cells were harvested by centrifugation at 4,400 × *g* for 10 min. Pellets were frozen until ready for processing. Labeled HCA II was prepared as described earlier (1). Isotopically labeled Tyr used for these experiments was uniformly ^{13}C- and ^{15}N-labeled tyrosine (CNLM-439-0.5; Cambridge Isotopes) or ζ-^{13}C–labeled tyrosine synthesized in-house.

NMR Spectroscopy Measurements and Assignments. ζ-^{13}C NMR signals were followed in directly observed ^{13}C spectra with ^{1}H decoupling on a sample of HCA II labeled with ζ-^{13}C–labeled tyrosine; 2 mM carnosine was added to the CA sample for pH monitoring and 0.1% DSS for spectral referencing. The pH dependence of carnosine resonances was determined in separate experiments. Several spectra were recorded on labeled HCA II in the pH range from 5.8 to 9.9 to determine pH-dependent chemical shift changes for Tyr signals. Data were processed using Mnova 9.0 software (Mestrelab Research) and chemical shifts were input into Origin7 (Microcal) for plotting and analysis. A plot of Tyr7 C_ζ chemical shift as a function of pH is shown in Fig. S1.

Residue-specific assignments of ζ-^{13}C carbons (Fig. S6) in tyrosine residues were obtained from a combination of 2D and 3D NMR experiments: ^{1}H-^{15}N HSQC, HNCACB, HBCB(CGCD)HD, HBCB(CGCDCE)HE, and aromatic HMBC using CA sample labeled with [U-^{13}C, ^{15}N]tyrosine (17). The experiments were recorded on 1.3 mM sample of labeled CA at pH 6.5 on a Bruker AVANCE III 700 MHz instrument equipped with a TCI cryoprobe and processed using TOPSPIN 3.2 software. ^{1}H-^{15}N HSQC cross-peaks were initially assigned using assignments obtained by Venters et al. (18). These were correlated with cross-peaks in HNCACB spectra to obtain corresponding C_β frequencies, which were correlated to H_δ and H_ε frequencies in HBCB(CGCD)HD and HBCB(CGCDCE)HE spectra. Using selective HMBC experiment yielded assignments for ζ-^{13}C carbons. The approach is illustrated in Fig. S7. Because of small chemical shift dispersion of C_β carbons and low resolution inherent in constant-time HBCB(CGCD)HD, HBCB(CGCDCE)HE experiments as well as missing peaks in HMBC spectra we could not unambiguously assign C_ζ carbons in Tyr51 and Tyr194.

Assignments of Tyr Cγ resonances were obtained using ^{1}H-^{15}N HSQC, HNCACB, ^{1}H-^{13}C HMQC, and CGCBHB (19) experiments, as shown in Fig. S5. Assignments of all C_β and C_γ carbon and H_β proton resonances were obtained. Tyrosine C_γ resonances were followed as a function of pH from 5.4 to 11.0 using a CGCBHB experiment. pH was monitored directly in the sample using a microelectrode. Spectra were processed using Bruker TOPSPIN 3.2 software and peak frequencies were input into Origin7 software for plotting and analysis. The integrity of the protein at pH 5.4, 6.7, and 11.0 was confirmed by recording ^{1}H-^{15}N HSQC spectra. At pH 11.48 the protein was mostly unfolded as evidenced by very limited signal dispersion in the spectrum. An overlay of CGCBHB spectra for Tyr7, Tyr88, and Tyr114 is shown in Fig. S7.

1. Fisher SZ, et al. (2009) Preliminary joint neutron and X-ray crystallographic study of human carbonic anhydrase II. *Acta Crystallogr Sect F Struct Biol Cryst Commun* 65(Pt 5):495–498.
2. Avvaru BS, et al. (2009) Apo-human carbonic anhydrase II revisited: Implications of the loss of a metal in protein structure, stability, and solvent network. *Biochemistry* 48(31):7365–7372.
3. Sentürk M, Gülçin I, Beydemir S, Küfrevioğlu OI, Supuran CT (2011) In vitro inhibition of human carbonic anhydrase I and II isozymes with natural phenolic compounds. *Chem Biol Drug Des* 77(6):494–499.
4. Minor W, Cymborowski M, Otwinowski Z, Chruszcz M (2006) HKL-3000: The integration of data reduction and structure solution—from diffraction images to an initial model in minutes. *Acta Crystallogr D Biol Crystallogr* 62(Pt 8):859–866.
5. Adams PD, et al. (2011) The Phenix software for automated determination of macromolecular structures. *Methods* 55(1):94–106.
6. Emsley P, Cowtan K (2004) Coot: Model-building tools for molecular graphics. *Acta Crystallogr D Biol Crystallogr* 60(Pt 12 Pt 1):2126–2132.
7. Coates L, Tomanicek S, Schrader TE, Weiss KL, Ng JD, Jüttner P, Ostermann A (2014) Cryogenic neutron protein crystallography: Routine methods and potential benefits. *J Appl Cryst* 47(4):1431–1434.
8. Niimura N, et al. (1994) An elastically bent silicon monochromator for a neutron diffractometer. *Nucl Instrum Methods A* 349:521–525.
9. Otwinowski Z, Minor W (1997) Processing of X-ray diffraction data collected in oscillation mode. *Methods in Enzymology*, eds Carter CW, Sweet RM (Academic, New York), Vol 276, pp 307–326.
10. Pflugrath JW (1999) The finer things in X-ray diffraction data collection. *Acta Crystallogr D Biol Crystallogr* 55(Pt 10):1718–1725.
11. Schoenborn BP, Langan P (2004) Protein crystallography with spallation neutrons. *J Synchrotron Radiat* 11(Pt 1):80–82.
12. Helliwell JR, et al. (1989) The recording and analysis of synchrotron X-radiation Laue diffraction photographs. *J Appl Cryst* 22:483–497.
13. Collaborative Computational Project, Number 4 (1994) The CCP4 suite: Programs for protein crystallography. *Acta Crystallogr D Biol Crystallogr* 50(Pt 5):760–763.
14. Adams PD, Mustyakimov M, Afonine PV, Langan P (2009) Generalized X-ray and neutron crystallographic analysis: More accurate and complete structures for biological macromolecules. *Acta Crystallogr D Biol Crystallogr* 65(Pt 6):567–573.
15. DeLano WL (2002) *The PyMOL Molecular Graphics System* (DeLano Scientific, San Carlos, CA).
16. Afonine PV, et al. (2012) Towards automated crystallographic structure refinement with phenix.refine. *Acta Crystallogr D Biol Crystallogr* 68(Pt 4):352–367.
17. Yamazaki T, Forman-Kay JD, Kay LE (1993) Two-dimensional NMR experiments for correlating 13 Cβ and 1 Hδ/ε chemical shifts of aromatic residues in 13 C-labeled proteins via scalar couplings. *J Am Chem Soc* 115:11054–11055.
18. Venters RA, Farmer BTII, 2nd, Fierke CA, Spicer LD (1996) Characterizing the use of perdeuteration in NMR studies of large proteins: 13C, 15N and 1H assignments of human carbonic anhydrase II. *J Mol Biol* 264(5):1101–1116.
19. Prompers JJ, Groenewagen A, Hilbers CW, Pepermans HAM (1998) Experiments for the assignment of aromatic side chains in ^{13}C-labeled proteins. *J Magn Reson* 130(Pt 1):68–75.

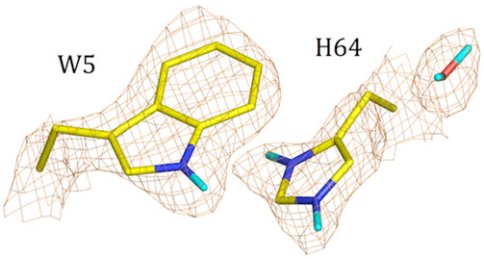

Fig. S1. Close-up view of His64 and Trp5 stacking interaction in *holo* pH 6 HCA II neutron structure. His64 is charged and in the "outward" conformation. The $2F_o - F_c$ nuclear density map is shown in blue mesh (contour 1.3σ). Exchanged Ds are in cyan; unexchanged H atoms are not shown for clarity. Active-site residues and solvent are as labeled. The nuclear density for Trp5 and His64 is shown in orange.

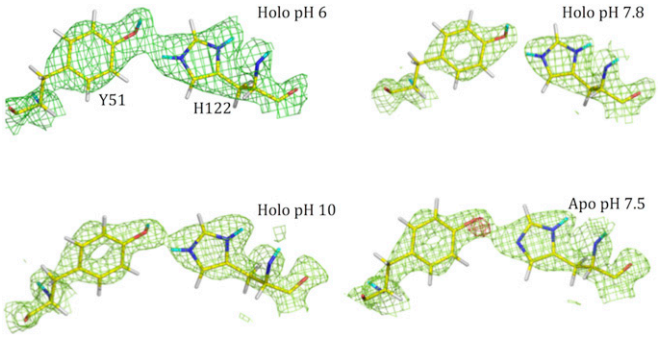

Fig. S2. Ball-and-stick representation of Tyr51 and interaction with His122 in the *holo* pH6, 7.8, and 10 and *apo* pH 7.8 neutron structures. $2F_o - F_c$ nuclear density map is shown in green mesh (contour 1.2 σ). Omit $F_o - F_c$ nuclear density is shown in red and is contoured at 3.5σ. Exchanged D atoms are shown in cyan, and unexchanged H atoms are show in white.

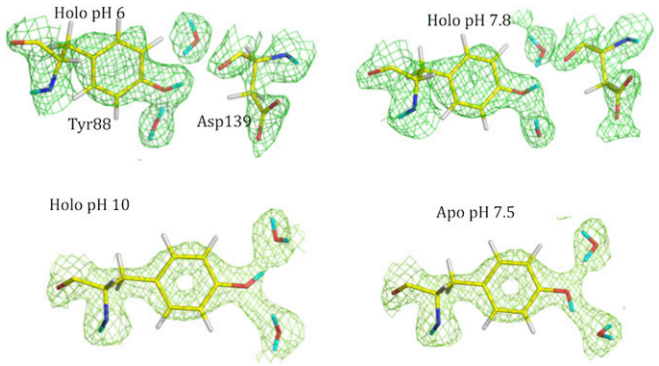

Fig. S3. Ball-and-stick representation of Tyr88 and interaction in the *holo* pH 6, 7.8, and 10 and *apo* pH 7.8 neutron structures. $2F_o - F_c$ nuclear density map is shown in green mesh (contour 1.2 σ). Exchanged D atoms are shown in cyan, and unexchanged H atoms are in white.

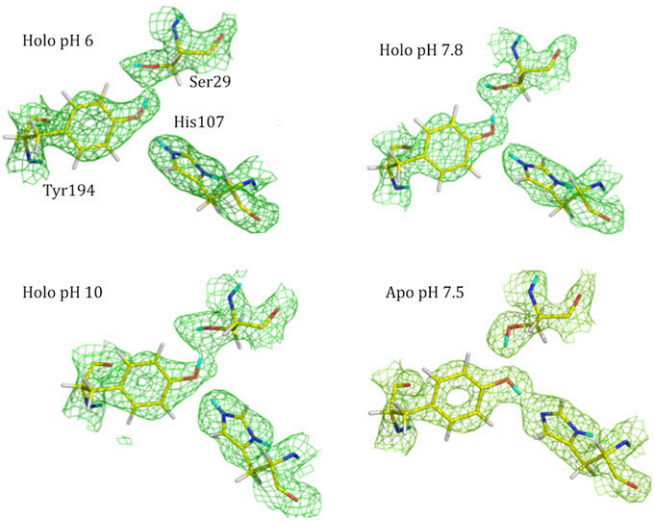

Fig. S4. Ball-and-stick representation of Tyr194 and interaction in the *holo* pH 6, 7.8, 10 and *apo* pH 7.8 neutron structures. $2F_o - F_c$ nuclear density map is shown in green mesh (contour 1.2 σ). Exchanged D atoms are shown in cyan, and unexchanged H atoms are in white.

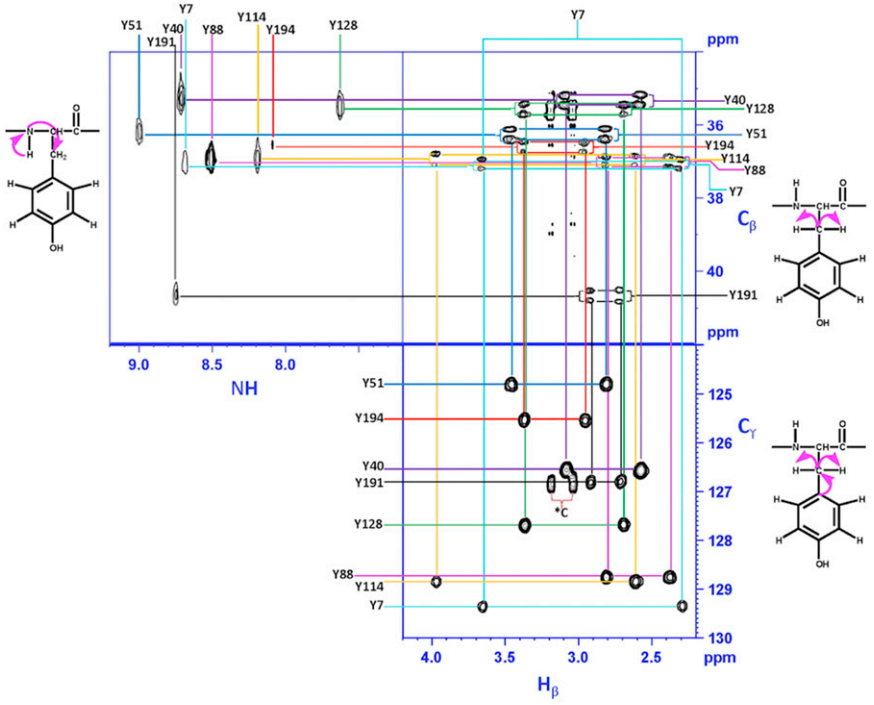

Fig. S5. NMR assignments of γ-^{13}C signals in labeled HCA II. Two bracketed cross-peaks in the lower right panel marked with *C are folded resonances from residual carnosine in the sample.

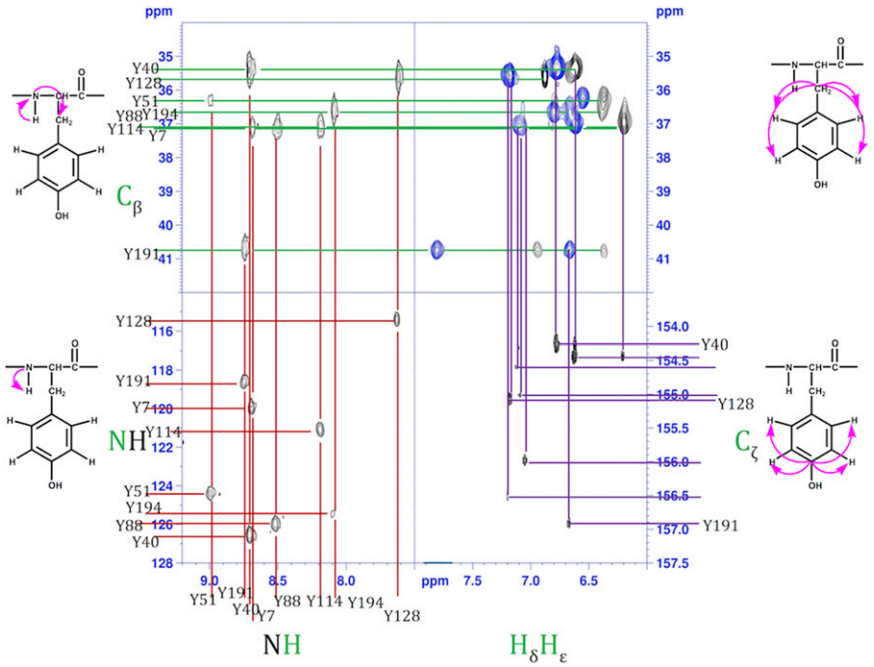

Fig. S6. NMR assignments of ζ-^{13}C signals in labeled HCA II.

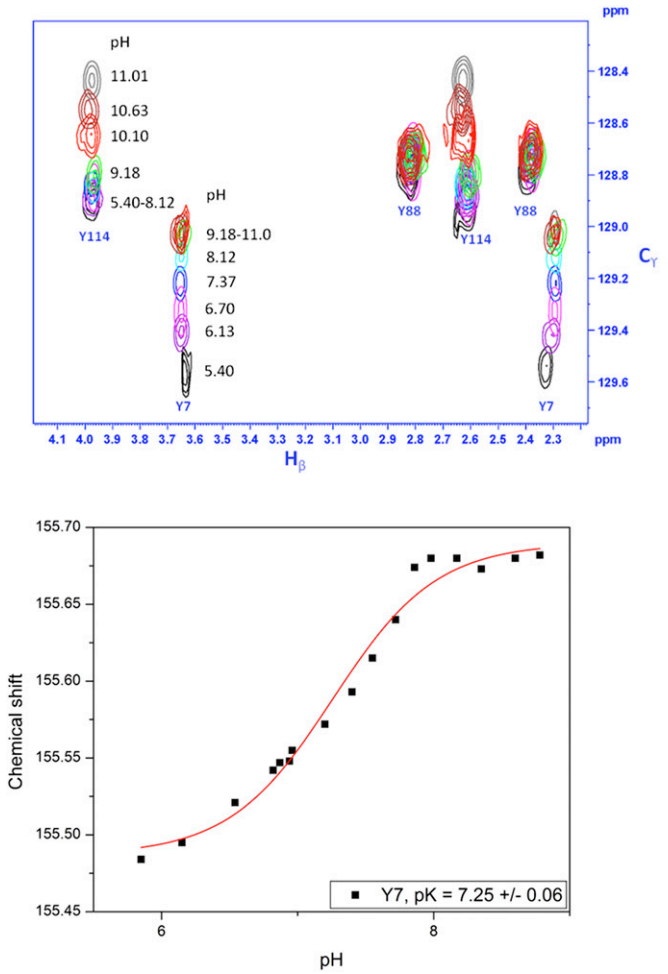

Fig. S7. Titration of Tyr7 as a function of pH. (*A*) Titration of Tyr7 followed in the 2D CGCBHB experiment. Also shown are resonances for Tyr88 and Tyr114. pH values for spectra are given next to the titrating resonances. Resonances for Tyr7 start shifting at low pH and stop above pH 8.12, whereas resonances for Tyr114 start shifting at pH 9.18. Chemical shift of Cγ resonances for Tyr88 remains essentially constant throughout entire pH range. (*B*) Tyr7 titration followed by chemical shift of ζ-^{13}C signals in labeled HCA II. Apparent pK_a value determined in this experiment is 7.25.

Table S1. Room-temperature X-ray and neutron data collection and refinement statistics

	Apo X-rays, neutrons pH 7.8	*Holo* neutrons pH 6
Wavelength, Å	1.54 (Cu Kα)/2.66	0.73–6.3 Laue
Space group	$P2_1$	$P2_1$
Unit cell, Å, °	a = 42.8, b = 41.7, c = 72.8, β = 104.7	a = 42.8, b = 41.7, c = 72.9, β = 104.7
No. of images, oscillations, °	120, 1°; 566, 0.35°	33 (no oscillation)
Resolution	30.0–1.60 (1.63–1.60); 30.0–1.80 (1.85–1.80)	25.0–2.00 (2.11–2.00)
No. of unique reflections	30,247 (1,061); 20,884 (1466)	13,799 (1,687)
Redundancy	2.5 (2.4); 2.7 (1.9)	2.7 (1.9)
Completeness, %	91.2 (65.3); 89.9 (76.8)	82.0 (70.0)
Mean I/sigma	16.7 (3.7); 6.5 (2.4)	4.5 (1.5)
R_{merge},† %	3.8 (31.8); 11.9 (33.0)	22.8 (38.2)
Joint R_{cryst}/R_{free},‡ %	17.9/18.8; 20.3/21.7	26.3/29.1

Values in parentheses are for the highest-resolution shell. *Holo* X-ray data were from the pH 6 room-temperature crystal structure with PDB ID code 1tbt.

†Rmerge = $(\sum | I - \langle I \rangle | / \sum \langle I \rangle) \times 100$.

‡Rcryst = $(\sum | Fo - Fc | / \sum |Fo|) \times 100$.